Ain Shams Engineering Journal (2014) 5, 1157–1166

Ain Shams University

Ain Shams Engineering Journal

www.elsevier.com/locate/asej
www.sciencedirect.com

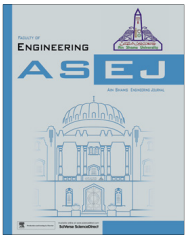

ELECTRICAL ENGINEERING

Dynamic modeling and performance evaluation of axial flux PMSG based wind turbine system with MPPT control

Vahid Behjat *, **Mehrdad Hamrahi**

Department of Electrical Engineering, Engineering Faculty, Azarbaijan Shahid Madani University, Tabriz, Iran

Received 23 February 2014; revised 4 May 2014; accepted 1 June 2014
Available online 15 July 2014

KEYWORDS

AFPMSG;
3D FEM;
Dynamic modeling;
Small-scale wind turbine;
MPPT

Abstract This research work develops dynamic model of a gearless small scale wind power generation system based on a direct driven single sided outer rotor AFPMSG with coreless armature winding. Dynamic modeling of the AFPMSG based wind turbine requires machine parameters. To this end, a 3D FEM model of the generator is developed and from magnetostatic and transient analysis of the FEM model, machine parameters are calculated and utilized in dynamic modeling of the system. A maximum power point tracking (MPPT)-based FOC control approach is used to obtain maximum power from the variable wind speed. The simulation results show the proper performance of the developed dynamic model of the AFPMSG, control approach and power generation system.

1. Introduction

Small-scale variable speed wind power generation systems have many advantages over fixed-speed generation such as availability, small size, high performances, low cost installation, operation at maximum power point and high power quality [1]. Various types of generators have been developed for wind turbine application. Because of the compact structure, high pole number, high power density and low weight of Axial Flux Permanent Magnet Synchronous Generator (AFPMSG), it is an excellent candidate for this purpose. One of the problems associated with the variable-speed wind systems is the presence of the gearbox coupling the wind turbine to the generator. The problem with the gearbox is that it suffers from considerable faults and also increases the maintenance expenses. Thus, in AFPMSG-based wind power generation systems the gearbox requirement is eliminated [2–4].

In variable speed wind turbines, the amount of delivered energy to the grid depends on the wind speed at the site and the generator rotor speed. The control strategy regulates the rotor speed based on the wind speed to absorb maximum power. Optimum power/torque tracking is a popular control strategy, as it helps to achieve optimum wind-energy utilization [5–9]. In these control strategies the information of the rotor position and speed is needed to implement the advanced control algorithms such as the field oriented control (FOC) [10] and direct torque control (DTC) [11].

* Corresponding author. Tel.: +98 9125963127.
E-mail address: Behjat@azaruniv.edu (V. Behjat).

Peer review under responsibility of Ain Shams University.

2090-4479 © 2014 Production and hosting by Elsevier B.V. on behalf of Ain Shams University.
http://dx.doi.org/10.1016/j.asej.2014.06.001

A literature review indicates that although, there are many research efforts dealing with simulations and experiments of wind energy conversion systems based on permanent magnet synchronous generators, but there are limited research works on axial flux PMSG. On the other side, the main research works on Axial-Flux PM Synchronous Generators are focused on design and optimization of these generators based on FEM modeling and simulations. Refs. [3,4,12–18] are dealing with electromagnetic and thermal design of Axial-Flux PM Synchronous Generators and developing some methods to optimize the back EMF and cogging torque of the machine using FE method. Wind power system modeling and control procedures in power generations with direct driven permanent magnet synchronous generators are discussed in [19–29]. This paper presents a detailed model of a gearless small scale wind power generation system based on a single sided outer rotor AFPMSG with coreless armature winding. Coreless type armature windings eliminate the armature iron loss, cogging torque and reduce magnetic pull between the field and the armature. Since the dynamic model of the AFPMSG needs the machine parameters, a 3D FEM model of the generator is developed and simulated. From magnetostatic and transient analysis of the 3D FEM model, generator parameters are calculated. Then these parameters are utilized in dynamic modeling of the AFPMSG. The considered generator is coupled to a small-scale variable speed wind turbine and a MPPT-based FOC control approach is used to regulate the speed of the generator to absorb maximum power from the wind turbine.

The paper is organized as follows: Section 2 presents dynamic modeling of the wind turbine. In Section 3, first the considered AFPMSG is modeled and simulated using 3D finite element method and then dynamic model of the generator is developed. The control system is described in Section 4. The results are analyzed and discussed in Section 5. Finally, Section 6 concludes the paper.

2. Wind turbine

The input wind power of the turbine is given by:

$$P_{wind} = \frac{E_{wind}}{t} = \frac{1}{2}\rho\pi R^2 V_w^3 \tag{1}$$

where ρ is the air density in (kg/m^3), R is the blade radius in (m), and V_w is wind speed in (m/s). The mechanical power and torque of the turbine are [8]:

$$P_{turbine} = \frac{1}{2}\rho\pi R^2 C_p(\lambda,\beta) V_w^3 \tag{2}$$

$$T_m = \frac{P_m}{\omega_m} = \frac{\frac{1}{2}\rho\pi R^2 C_p(\lambda,\beta) V_w^3}{\omega_m} \tag{3}$$

where C_p is the turbine efficiency in converting wind energy to mechanical energy which is obtained from the following equations [24]:

$$C_p = c_1\left(c_2\frac{1}{\alpha} - c_3\beta - c_4\beta^x - c_5\right)e^{-c_6\frac{1}{\alpha}} \tag{4}$$

$$\frac{1}{\alpha} = \frac{1}{\lambda + 0/08\beta} - \frac{0/035}{1+\beta^3} \tag{5}$$

$$\lambda = \frac{\omega_m R}{V_w} \tag{6}$$

where λ and β are the tip speed ratio and pitch angle of the blades, respectively. The value of the c_1–c_6 coefficients depend on the type of the turbine [26]. ω_m is the mechanical angular speed of the turbine in (rad/s) which in turn is obtained from the following equation:

$$T_e - T_m = J\frac{d}{dt}\omega_m + B\omega_m \tag{7}$$

where T_e and T_m are the electromagnetic and mechanical torque, respectively. J is the combined inertia of the rotor and the wind turbine in (kg m^2). B is the viscous friction of the rotor in $\left(\frac{N.m.s}{rad}\right)$. Based on the described equations from (1)–(7), the dynamic model of the wind turbine is depicted in Fig. 1.

3. AFPMSG

The axial flux generator used in this study which is connected to the wind turbine system, is an outer-rotor single sided AFPMSG with 3 phase star connected stator winding. Fig. 2a and b illustrate the geometrical and winding arrangement of the considered generator. As it can be shown in Fig. 2, the rotor of the considered single sided AFPMSG has two disks in order to decrease the axial forces between the rotor and the stator, but the permanent magnets are assembled on just one of the disks.

Electromechanical and geometrical data of the considered generator are summarized in Tables 1 and 2 respectively. The permanent magnets used in the generator are NdFeB magnets with Br = 1.13 [T], Hc = 796 [kA/m] and $(BH)_{max}$ = 119 [kJ/mˆ3] and maximum operating temperature of 140 [°C].

3.1. 3D FEM model of AFPMSG

Dynamic modeling of the AFPMSG needs electrical parameters of the machine. In this section, these parameters are calculated through a 3D FEM model of the considered AFPMSG. In the three-dimensional (3D) problem considered here for the electromagnetic analysis of the studied AFPMSG, the electromagnetic field and circuit-coupled approach based on the A-V-A formulation is used. From the well-known Maxwell's equations, the computation of the magnetic field, based on the A-V-A formulation with the Coulomb gauge, leads to the following equation:

$$\nabla\times([\nu]\nabla\times\vec{A}) - \nabla\nu_e\nabla\cdot\vec{A} = \vec{J} \tag{8}$$

$$-\nabla\cdot[\sigma]\left(\frac{\partial\vec{A}}{\partial t} + \nabla V\right) = \nabla\cdot J = 0 \tag{9}$$

The governing equation in the permanent magnet region is described as follows:

$$\nabla\times([\nu]\nabla\times\vec{A}) - \nabla\nu_e\nabla\cdot\vec{A} = \nabla\times\left(\frac{[\nu][\vec{M_0}]}{\nu_0}\right) \tag{10}$$

where $\vec{A}$ and V are the magnetic vector potential and scalar electric potential respectively. $[\nu]$ is the reluctivity matrix and $[\sigma]$ is the conductivity matrix. ν_e is defined as one-third of the reluctivity matrix. $\vec{J}$ is the current density, $\vec{M_0}$ is the

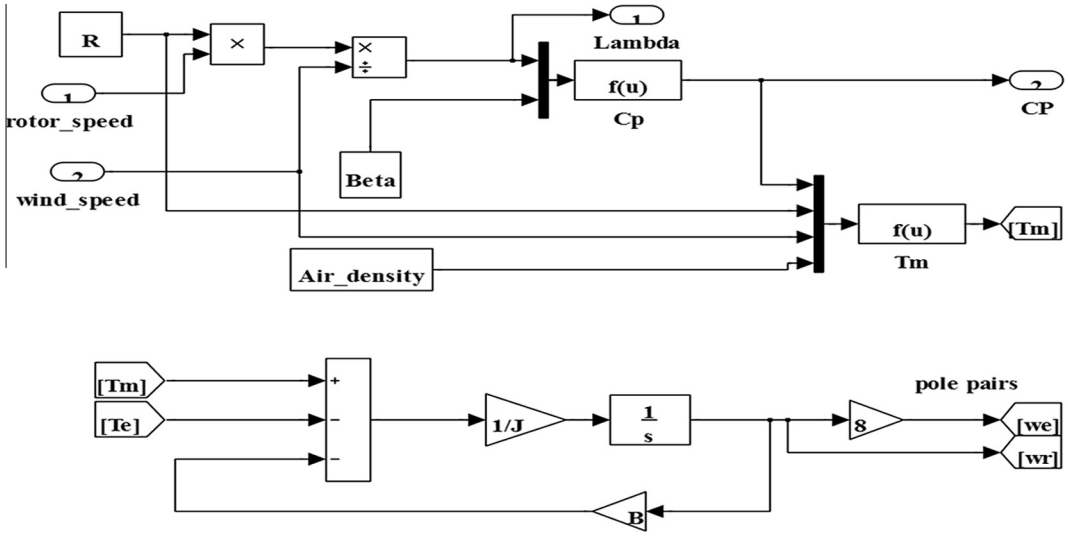

Figure 1 Dynamic model of the wind turbine.

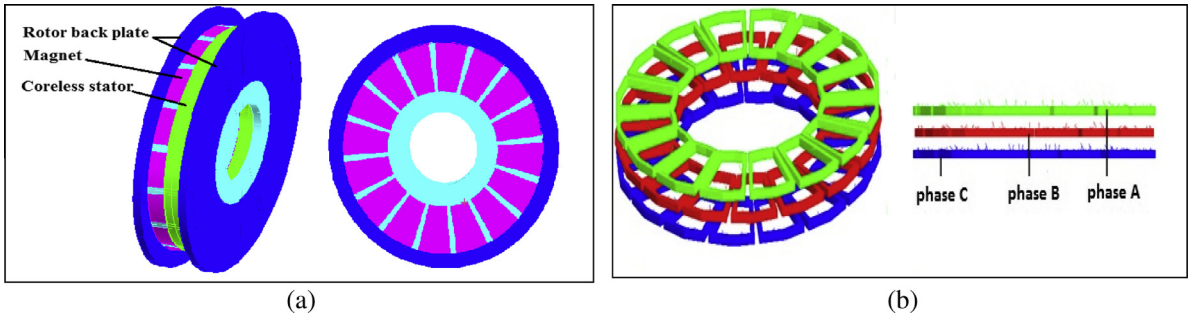

Figure 2 (a) Full geometrical model of the considered AFPMSG, (b) winding arrangement.

Table 1 Electromechanical data of the considered AFPMSG.

Parameter	Value
Rated Frequency	60 (Hz)
Electrical power in rated speed	230 (w)
Pole pairs	8
Number of phases	3
Number of coils/phase	7
Rated speed	450 (rpm)

remanent intrinsic magnetization vector and v_0 is the reluctivity of the free space [13].

Full meshed model of the considered generator is illustrated in Fig. 3. As it can be shown in the figure, square elements have been used in the radial and rotational directions, while triangle surface elements are implemented in the Z-direction. Because of the magnetic field strength between the poles, the greater number of elements is used in the region.

Flux density distribution in rotor back plates of the generator is depicted in Fig. 4. Due to symmetry of the AFPMSG, only two poles have been used to illustrate the flux distribution in the generator.

Fig. 5a and b illustrate the no-load voltage and short circuit current of the considered generator respectively which are obtained from the 3D FEM transient simulation.

In the considered generator, the inductances expressed in the quadrature coordinates have the same values equal to the synchronous inductance ($L_d = L_q = L_s$). The synchronous inductance is determined from the synchronous reactance ($X_s = L_s\omega$) which in turn is obtained from the no-load line voltage and short circuit current of the generator in the rated speed condition, as follows:

Table 2 Geometrical data of the considered AFPMSG.

Machine part	Inner radius (mm)	Outer radius (mm)	Axial thickness (mm)
Rotor back plate (one part)	55	115	5
Winding	45	110	5
Magnet	55	100	6
Active air gap	45	110	2×0.7

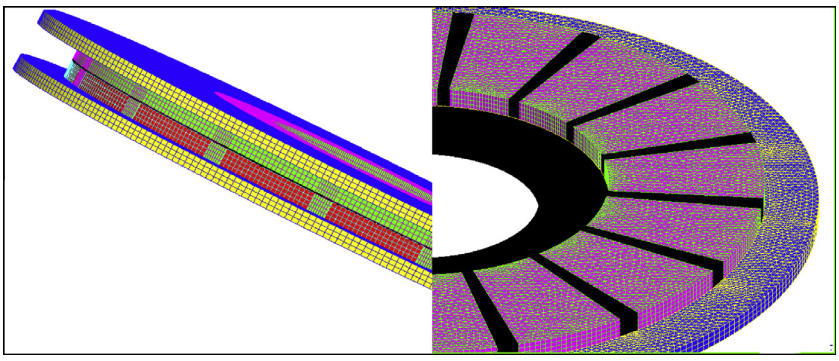

Figure 3 Full meshed model of the considered AFPMSG.

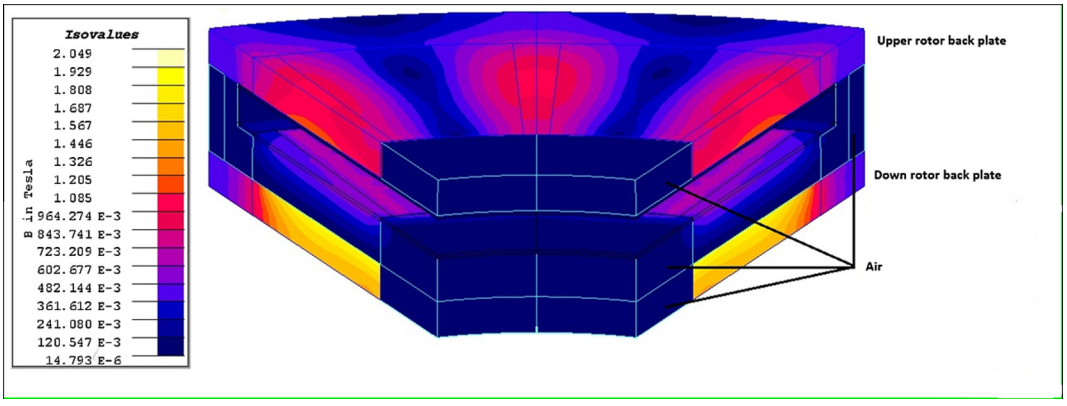

Figure 4 Flux density distribution on rotor back plates.

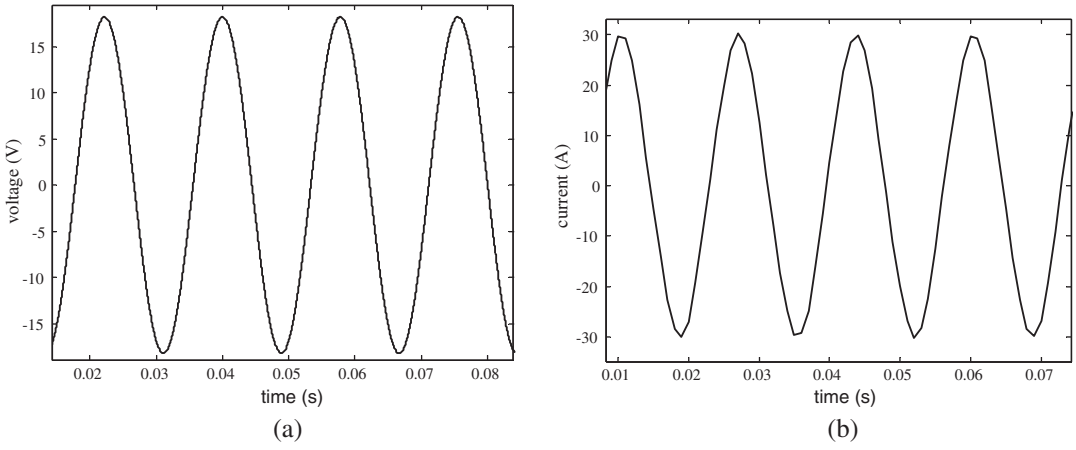

Figure 5 Electrical signals from FEM transient simulation: (a) no load voltage, (b) short circuit current.

$$Z_s = \frac{V_{L-noload}}{\sqrt{3} I_{SC}} \tag{11}$$

$$X_s = \sqrt{Z_s^2 - R_s^2} \tag{12}$$

$$L_s = \frac{X_s}{\omega} \tag{13}$$

In the above equations, R_s is the stator windings resistance and $V_{L\text{-}noload}$ and I_{SC} are no-load line voltage and short circuit current of the considered generator at rated speed (450 rev/min) respectively which were previously obtained from the FEM computations. The calculated inductances are used in dynamic modeling of the AFPMSG in next section.

3.2. Dynamic modeling of AFPMSG

Based on the 3D FEM results and electrical machinery equations, a dynamic model is developed for the considered AFPMSG in this section. The AFPMSG is normally modeled

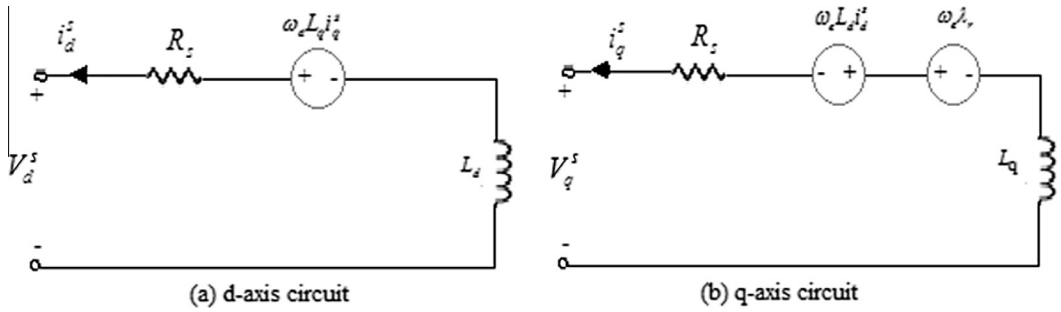

Figure 6 *d–q*-Axes equivalent circuits of the AFPMSG.

in the rotor field (*dq*-axis) synchronous reference frame, where the *q*-axis is 90 degree ahead of the *d*-axis with respect to the direction of rotation. The flux caused by the PM is in direction of the *d*-axis. Stator voltage equations are described as follows:

$$\vec{V}^s_{abc} = R_s \vec{I}^s_{abc} + \frac{d}{dt}\vec{\lambda}^s_{abc} \tag{14}$$

where $\vec{V}^s_{abc}$ is the stator phase voltages, $\vec{I}^s_{abc}$ is the stator phase currents, $\vec{\lambda}^s_{abc}$ is the flux linkages and R_s is the stator phase winding resistances. With some simplifications, *dq* coordinate frame equations arranged as below:

$$V^s_d = -R_s i^s_d - \omega_e \lambda^s_q + \frac{d}{dt}\lambda^s_d \tag{15}$$

$$V^s_q = -R_s i^s_q + \omega_e \lambda^s_d + \frac{d}{dt}\lambda^s_q \tag{16}$$

Flux linkage equations are:

$$\lambda^s_d = -L_d i^s_d + \lambda_r \tag{17}$$

$$\lambda^s_q = -L_q i^s_q \tag{18}$$

where V^s_d and V^s_q are the *d–q* axes stator voltages, i^s_d and i^s_q are the *d–q* axes stator currents, λ^s_d and λ^s_q are the *d–q* axis stator flux linkages, and ω_e is the rotor mechanical speed. λ_r is the permanent magnet flux which is constant in the considered AFPMSG.

With substituting (15) and (16) in (17) and (18), the voltage equations are modified to:

$$V^s_d = -R_s i^s_d + \omega_e L_q i^s_q - L_d \frac{d}{dt} i^s_d \tag{19}$$

$$V^s_q = -R_s i^s_q - \omega_e L_d i^s_d + \omega_e \lambda_r - L_q \frac{d}{dt} i^s_q \tag{20}$$

Equivalent circuits of the AFPMSG based on (19) and (20) equations are illustrated in Fig. 6.

Mathematical model of the APMSG is completed with the developed electromagnetic torque equation which is described by the following:

$$T_e = \frac{3p}{2}\left(i^s_q \lambda^s_d - i^s_d \lambda^s_q\right) = \frac{3p}{2}\left[i^s_q \lambda_r - (L_d - L_q) i^s_d i^s_q\right] \tag{21}$$

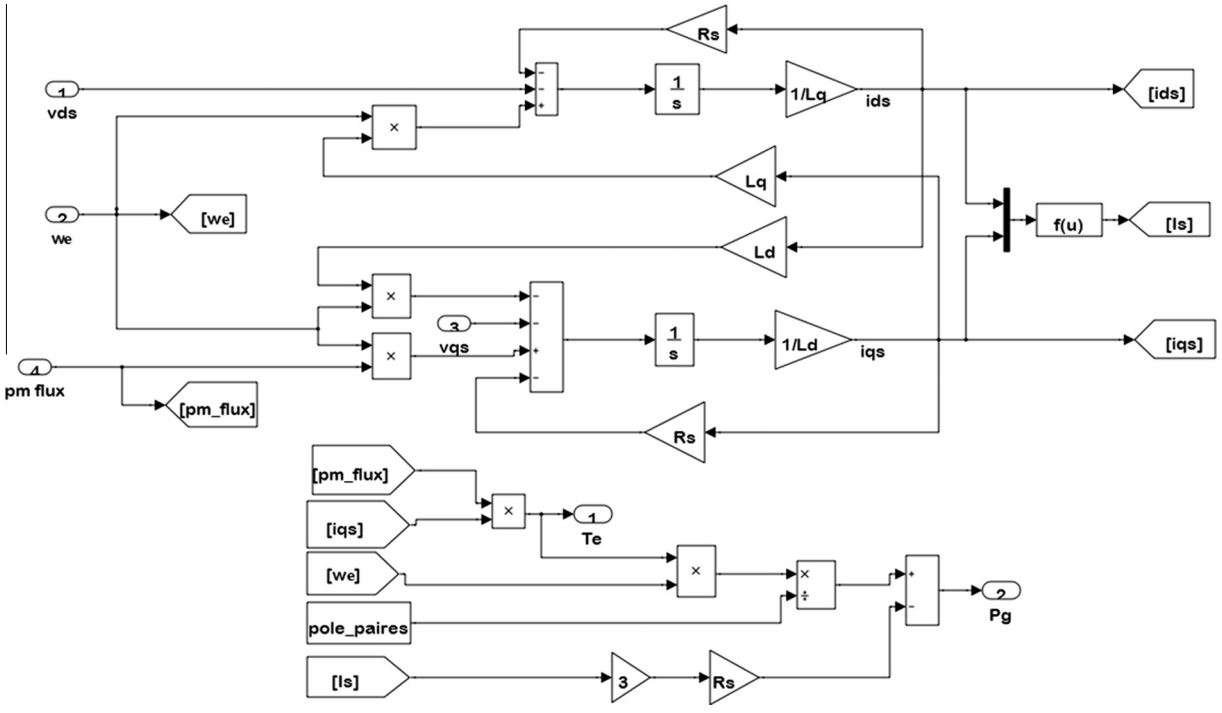

Figure 7 Dynamic model of the considered AFPMSG.

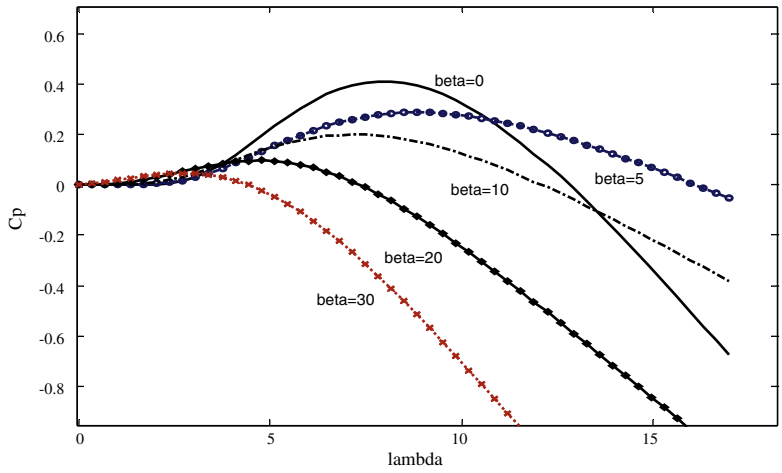

(a)

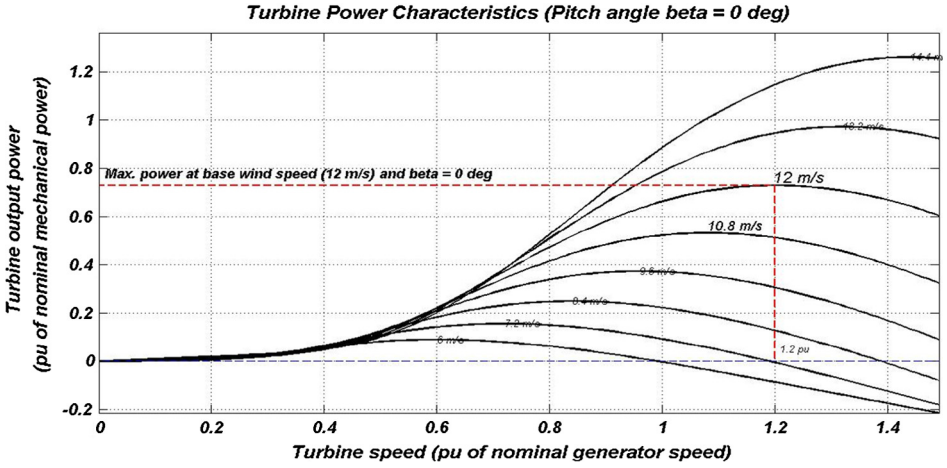

(b)

Figure 8 (a) C_p variations versus λ and β, (b) turbine output power versus generator speed with the wind speed as a parameter.

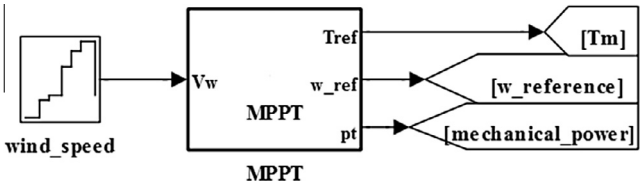

Figure 9 MPPT input and output.

In AFPM machines, the flux caused by PM is constant and supposed to be in direction of the d-axis. Hence λ_q^s term is omitted from the electromagnetic torque equation. Also, considering that the d and q axes inductances have the same values ($L_d = L_q$), Eq. (21) is modified to:

$$T_e = \frac{3p}{2} i_q^s \lambda_r \tag{22}$$

The d–q axes current equations are described as following:

$$i_d^s = \frac{1}{S}\left(-V_d^s - R_s i_d^s + \omega_e L_q i_q^s\right) \Big/ L_d \tag{23}$$

$$i_q^s = \frac{1}{S}\left(-V_q^s - R_s i_q^s - \omega_r L_d i_d^s + \omega_e \lambda_r\right) \Big/ L_q \tag{24}$$

Since the considered AFPMSG in this study has not stator core, so the machine losses are limited to the resistive loss in the stator three phase windings. Therefore, the power that is delivered to the load can be expressed as:

$$P_S = P_m - P_{cus} = T_e \frac{\omega_e}{p} - 3R_s I_S^2 \tag{25}$$

which

$$I_S = \sqrt{i_d^{s2} + i_q^{s2}} \tag{26}$$

Based on the above described equations, the dynamic model of the considered AFPMS is illustrated in Fig. 7.

4. Control system

Fig. 8a illustrates the turbine power coefficient versus tip speed ratio in different values of the pitch angle of the blades. Variation in the turbine output power against the rotor speed in different values of the wind speed is depicted in Fig. 8b. As can be easily seen from the figures, a maximum power coefficient exists at any wind speed. Therefore a control system, called MPPT, is needed to regulate the speed of the generator in order to absorb maximum power from the turbine.

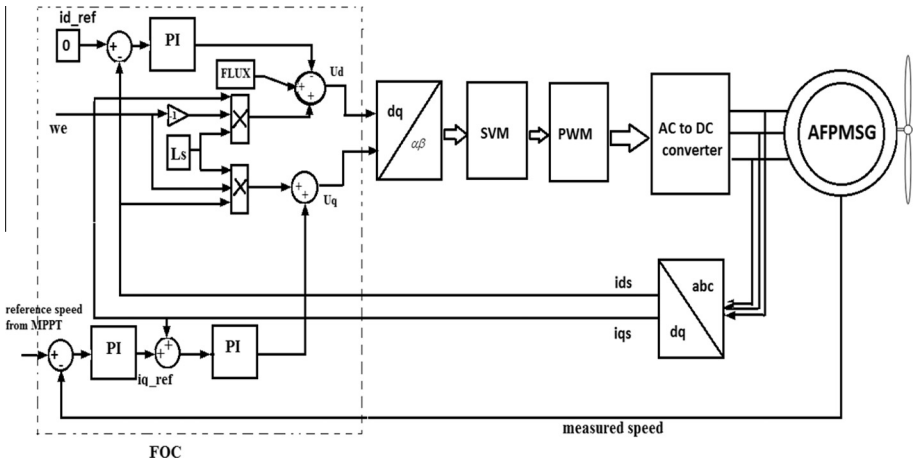

Figure 10 Power generation system with implemented control strategy.

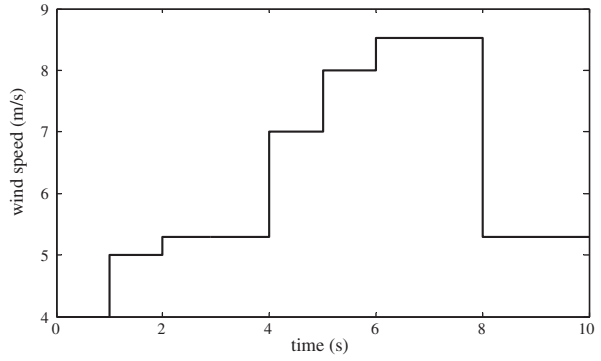

Figure 11 Imposed wind speed.

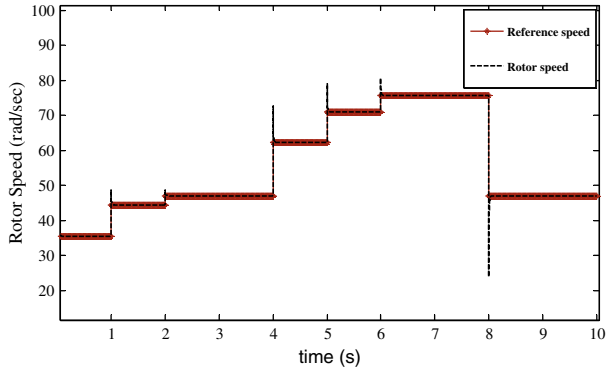

Figure 12 Rotor reference and measured speed.

Based on this rotor reference speed, ω_{m_ref}, the reference values of the mechanical power and torque are obtained as below:

$$P_{m\_ref} = \frac{1}{2}\rho\pi R^2 C_{pmax} V_w^3 \tag{27}$$

$$T_{m\_ref} = \frac{\frac{1}{2}\rho\pi R^2 C_{pmax} V_w^3}{\omega_{m\_ref}} \tag{28}$$

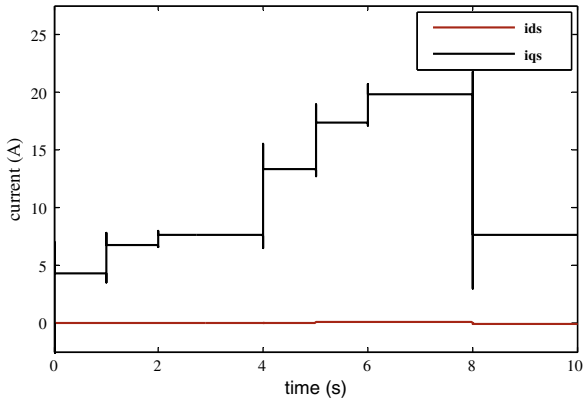

Figure 13 *d–q* Axes currents.

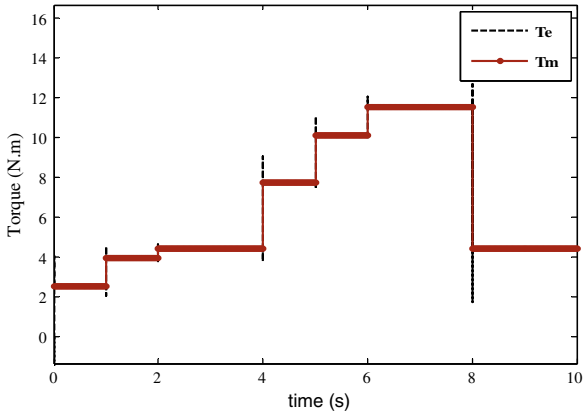

Figure 14 Mechanical and electromagnetic Torque.

Fig. 9 represents a simple block diagram of the MPPT control system. As it is obvious from the figure, from the MPPT control, the rotor reference speed is carried out and then this reference value is utilized as input of the AFPMSG dynamic model. As illustrated in Fig. 9, this MPPT method has one input signal and so it has less computation and more performance. The steady-state-induced voltage and torque equations of the AFPMSG are given by:

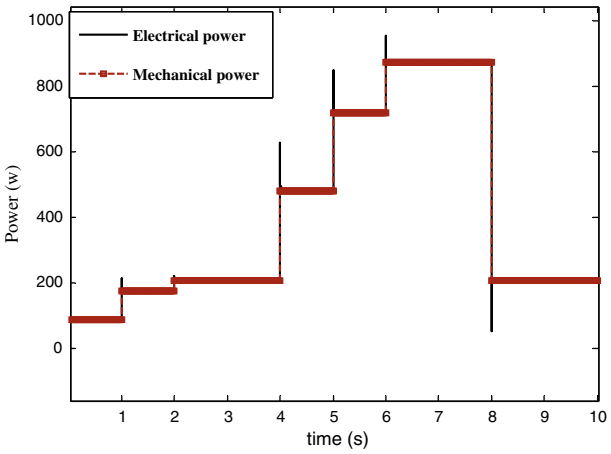

Figure 15 Mechanical and electric power.

$$T = K_t I \tag{29}$$

$$E = K_e \omega \tag{30}$$

where ω is the rotor speed and I is the stator current. Also, we have:

$$E^2 = V^2 + (I\omega L_S)^2 \tag{31}$$

where V is the terminal voltage of the AFPMSG and Ls is its winding phase inductance. The rectified dc value of the output voltage may be obtained using:

$$V_{dc} = \frac{3\sqrt{6}}{\pi} V \tag{32}$$

Using Eqs. (30)–(32), the rectified dc voltage may be written as:

$$V_{dc} = \frac{3\sqrt{6}}{\pi} \omega \sqrt{K_e^2 - \left(\frac{TL_S}{K_t}\right)^2} \tag{33}$$

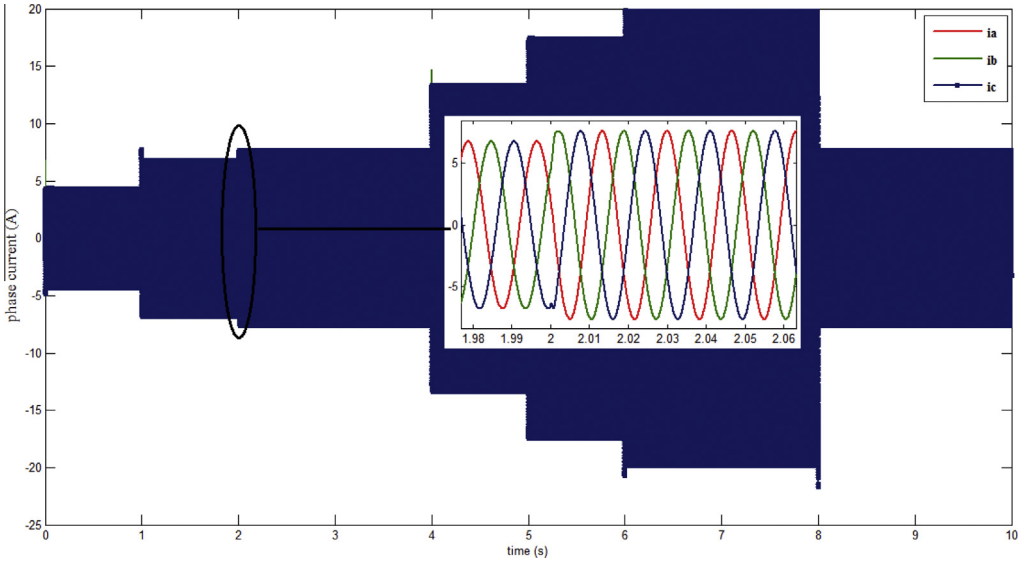

Figure 16 Three phase currents of the AFPMSG.

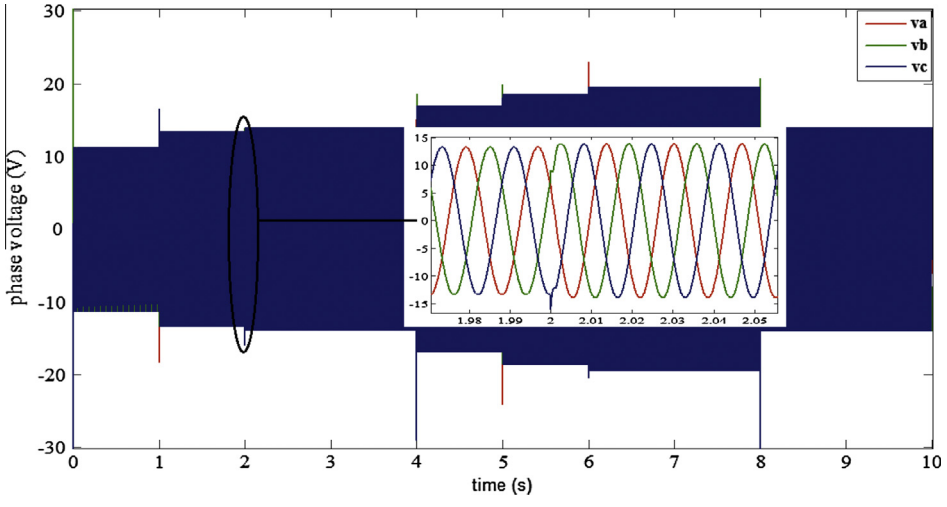

Figure 17 Three phase voltages of the AFPMSG.

The torque is determined by the generator speed and the wind speed, therefore according to (33), it is possible to obtain a prediction for the *dc* voltage as a function of the generator speed and the wind speed. As a result, the generator speed can be regulated by setting the *dc* voltage. Using rotor speed feedback, the optimum rectified *dc* voltage is specified. Using new optimum *dc* voltage, AFPMSG rotor speed will change and a new *dc* voltage command is specified from Eq. (33). With this control strategy, generator rotor speed and *dc* voltage are continuously changed until an equilibrium point is reached [30].

To control the AFPMSG speed and hence power generation, the field oriented control (FOC) is used in this paper. In the FOC approach, the *dq*-axes are rotating at the rotor electrical angular speed with the *d*-axis aligned on the rotor flux direction. Thus, the flux producing current component, i_d^s, and the torque producing current component, i_q^s, are along the *d*-axis and *q*-axis, respectively. Therefore, the *dq*-axes currents can be controlled independently by two closed loop controls in the FOC approach to control the speed and the torque of the AFPMSG. The FOC approach is coupled to the optimum tip speed ratio based MPPT control strategy. The implemented control system is illustrated in Fig. 10. As can obviously seen from the figure, the measured rotor speed is compared with its reference value which has been extracted from the MPPT strategy, and then the reference *q*-axis current of the AFPMSG, i_{q_ref}, is obtained with regulation of the PI coefficients. Zero reference current is assigned to the direct component of the stator current, i_{d_ref}, to achieve maximum torque/ampere capability.

5. Simulation results

In this section, simulation results are provided in order to evaluate the effectiveness of the developed dynamic model of the AFPMSG-based small-scale wind power generation. In order to observe the power generated by the wind turbine and AFPMSG, a linear wind profile (Fig. 11) is imposed to simulate the model. Considering the MPPT control algorithm, the resulting reference rotor speed and measured rotor speed are illustrated in Fig. 12.

The *d* and *q* axes currents of the AFPMSG are illustrated in Fig. 13. As can be obviously seen from the figure, the direct axis current (i_{ds}) is approximately zero and follows its reference value (i_{ds}^*) closely. This proves that the maximum value of the electrical torque is achieved in different wind speeds according to the implemented control strategy.

The electromagnetic torque of the AFPMSG is compared with the reference mechanical torque in Fig. 14. Fig. 15 illustrates the AFPMSG generated active electric power and the applied mechanical power to the AFPMSG.

The terminal currents and voltages of the generator are illustrated in Figs. 16 and 17 respectively.

Rapid convergence of angular rotor speed and output electric power of the AFPMSG to their reference values proves the good performance of the control system which utilizes the MPPT control strategy. Considering the simulation results, one can conclude that the developed system operates well, fulfilling the imposed requirements, i.e. extracting the maximum power from the wind turbine and converting it to the active electric power for delivering to the consumer.

6. Conclusion

This research work developed a dynamic model for a gearless small scale wind power generation system based on a single sided outer rotor AFPMSG with coreless armature winding. A 3D FEM model of the considered generator was developed and simulated in both magnetostatic and transient conditions to obtain the machine parameters which are required for dynamic modeling of the system. The considered generator was coupled to a variable speed wind turbine and a MPPT-based FOC control approach was utilized to regulate the speed of the generator to absorb maximum power from the wind turbine. Simulation results verified the proposed model of the AFPMSG, control system and MPPT approach. The developed model can be used for investigating dynamic behavior of AFPM machines and small scale power generation systems.

References

[1] Chen Z, Guerrero J, Blaabjerg F. A review of the state of the art of power electronics for wind turbines. IEEE Trans Power Electron 2009;24(8):1859–75.

[2] Gieras JF, Wang RJ, Kamper MJ. Axial flux permanent magnet brushless machine. Dordrecht: Kluwer Academic Publisher; 2004.

[3] Brisset Stéphane, Vizireanu Darius, Brochet Pascal. Design and optimization of a nine-phase axial-flux PM synchronous generator with concentrated winding for direct-drive wind turbine. IEEE Trans Ind Appl 2008;44(3).

[4] Di Gerlando Antonino, Foglia Gianmaria, Iacchetti Matteo Felice, Perini Roberto. Axial flux pm machines with concentrated armature windings: design analysis and test validation of wind energy generators. IEEE Trans Ind Electron 2011;58(9).

[5] De Broe M, Drouilhet S, Gevorgian V. A peak power tracker for small wind turbines in battery charging applications. IEEE Trans Energy Convers 1999;14(4):1630–5.

[6] Datta R, Ranganathan VT. A method of tracking the peak power points for a variable speed wind energy conversion system. IEEE Trans Energy Convers 1999;18(1):163–8.

[7] Tan K, Islam S. Optimal control strategies in energy conversion of PMSG wind turbine system without mechanical sensors. IEEE Trans Energy Convers 2004;19(2):392–9.

[8] Morimoto S, Nakayama H, Sanada M, Takeda Y. Sensorless output maximization control for variable-speed wind generation system using IPMSG. IEEE Trans. Ind. Appl. 2005;41(1):60–7.

[9] Chinchilla M, Arnaltes S, Burgos JC. Control of permanent magnet generators applied to variable-speed wind-energy systems connected to the grid. IEEE Trans Energy Convers 2006;21(1):130–5.

[10] Blaschke Felix. The principle of field orientation as applied to the new TRANSVECTOR closed loop control system for rotating field machines. Siemens Rev 1972;34(5):217–20.

[11] Takahashi I, Ohmori Y. High-performance direct torque control of an induction motor. IEEE Trans Ind Appl 1989;25:257–64.

[12] Chan TF, Lai LL. An axial-flux permanent-magnet synchronous generator for a direct-coupled wind-turbine system. IEEE Trans Energy Conver 2007;22(1):86–94.

[13] Chan TF, Wang Weimin, Lai LL. Performance of an axial-flux permanent magnet synchronous generator from 3-d finite-element analysis. IEEE Trans Energy Convers 2010;25(3).

[14] Sadeghierad M, Darabi A, Lesani H, Monsef H. Optimal design of the generator of microturbine using genetic algorithm and PSO. Electr Power Energy Syst 2010;32:804–8.

[15] Roberto Di Stefanon, Marignetti Fabrizio. Electromagnetic analysis of axial-flux permanent magnet synchronous machines with fractional windings with experimental validation. IEEE Trans Ind Electr 2012;59(6).

[16] Choi Jang-Young, Lee Sung-Ho, Ko Kyoung-Jin, Jang Seok-Myeong. Improved analytical model for electromagnetic analysis of axial flux machines with double-sided permanent magnet rotor and coreless stator windings. IEEE Trans Mag 2011;47(10).
[17] Gonzalez DA, Tapia Juan A, Bettancourt AL. Design consideration to reduce cogging torque in axial flux permanent-magnet machines. Trans Mag 2007;43(8).
[18] Virtic Peter, Pisek Peter, Hadziselimovic Miralem, Marcic Tine, Stumberger Bojan. Torque analysis of an axial flux permanent magnet synchronous machine by using analytical magnetic field calculation. IEEE Trans Mag 2009;45(3).
[19] Reis MM, Soares B, Barreto LHSC, Freitas E, Silva CEA, Bascopé RT, Oliveira Jr DS. A variable speed wind energy conversion system connected to the grid for small wind generator. In: Proc. of 23rd an. conf. of IEEE applied power electronics, APEC – 2008. Austin; 24–28 February 2008. P. 751–5.
[20] Rolan Alejandro, Luna Alvaro, Vazquez Gerardo, Aguilar Daniel, Azevedo Gustavo. Modeling of a variable speed wind turbine with a permanent magnet synchronous generator. IEEE (ISlE 2009). Korea; July 5–8, 2009.
[21] Drugă M, Nichita C, Barakat G. Performances Study of Direct coupled PM Generator based Small Wind Converters. XIX ICEM; 2010.
[22] Teodorescu R, Blaabjerg F. Flexible control of small wind turbines with grid failure detection operating in stand-alone and grid-connected mode. IEEE Trans Power Electr 2004;19(5):1323–32.
[23] Haque Md Enamul, Negnevitsky Senior Michael, Muttaqi Kashem M. A novel control strategy for a variable-speedwind turbine with a permanent-magnet synchronous generator. IEEE Trans Ind Appl 2010;46(1):331–9.
[24] Sun T, Chen Z, Blaabjerg F. Voltage recovery of grid-connected wind turbines after a short-circuit fault. In: Proc of the 29th Annual Conference of the IEEE Industrial Electronics Society, vol. 3; June 20–25, 2004. p. 827–31.
[25] Timbus Adrian, Liserre Marco, Teodorescu Remus, Rodriguez Pedro, Blaabjerg Frede. Evaluation of current controllers for distributed power generation systems. IEEE Trans Power Electron 2009;24(3).
[26] Heier S. Grid integration of wind energy conversion systems. John Wiley & Sons Ltd; 1998 [ISBN 0-471-97143-X].
[27] Orlando NA, Liserre M, Monopoli VG, Mastromauro RA, Dell'Aquila A. Comparison of power converter topologies for permanent magnet small wind turbine system. In: IEEE international symposium on industrial electronics, ISIE 2008. Cambridge; June 30 2008–July 2008. p. 2359–64.
[28] Malesani L, Tenti P. A novel hysteresis control method for current-controlled voltage-source PWM inverters with constant modulation frequency. IEEE Trans Ind Appl 1990;26:88–92.
[29] Bord DM, Novotony DW. Current control of VSI-PWM inverters. IEEE Trans Ind Appl 1985;21:562–70.
[30] Dehghan Seyed Mohammad, Mohamadian Mustafa, Varjani Ali Yazdian. A new variable-speed wind energy conversion system using permanent-magnet synchronous generator and z source inverter. IEEE Trans Energy Convers 2009;24(3).

Vahid Behjat was born in 1980 in Tabriz, Iran. He received the B.Sc. degree in Electrical Engineering from University of Tabriz, Tabriz, Iran, in 2002, and the M.Sc. and Ph.D. degrees in Electrical Engineering from Iran University of Science and Technology, Tehran, Iran, in 2002 and 2010, respectively. Currently, he is an Assistant Professor in Department of Electrical Engineering, Azarbaijan Shahid Madani University, Tabriz, Iran. His main research interests include design and modeling of electrical machines, diagnostics and condition monitoring of power transformers and electrical machines, and application of finite-element method to design, model, and optimization of electrical machines.

Mehrdad Hamrahi was born in Iran, on January 1986. He received the B.Sc. degree in control and electrical engineering from Tabriz University, Iran, in 2010 and M.Sc. degree in electrical engineering, from Azarbaijan Shahid Madani University, Tabriz, Iran, in 2014. His research interests include electric machinery design, modeling and analysis of electric machines, renewable energy systems and power system control.